Title

Molecular Dynamics and Monte Carlo simulations resolve apparent diffusion rate differences for proteins confined in nanochannels

Authors

Tringe, JW
Ileri, N
Levie, HW
et al.

Publication Date

2015-08-01

DOI

10.1016/j.chemphys.2015.04.021

Peer reviewed

Chemical Physics 457 (2015) 19–27

Contents lists available at ScienceDirect

Chemical Physics

journal homepage: www.elsevier.com/locate/chemphys

Molecular Dynamics and Monte Carlo simulations resolve apparent diffusion rate differences for proteins confined in nanochannels

J.W. Tringe [a,*], N. Ileri [a,b], H.W. Levie [a], P. Stroeve [b], V. Ustach [b], R. Faller [b], P. Renaud [c]

[a] Lawrence Livermore National Laboratory, 7000 East Avenue, Livermore, CA, USA
[b] Department of Chemical Engineering & Materials Science, University of California, Davis, CA, USA
[c] Swiss Federal Institute of Technology, Lausanne, (EPFL), Switzerland

ARTICLE INFO

Article history:
Received 26 December 2014
In final form 24 April 2015
Available online 18 May 2015

Keywords:
Molecular Dynamics
Monte Carlo
Nanochannel
Protein
Nanopore
Membrane

ABSTRACT

We use Molecular Dynamics and Monte Carlo simulations to examine molecular transport phenomena in nanochannels, explaining four orders of magnitude difference in wheat germ agglutinin (WGA) protein diffusion rates observed by fluorescence correlation spectroscopy (FCS) and by direct imaging of fluorescently-labeled proteins. We first use the ESPResSo Molecular Dynamics code to estimate the surface transport distance for neutral and charged proteins. We then employ a Monte Carlo model to calculate the paths of protein molecules on surfaces and in the bulk liquid transport medium. Our results show that the transport characteristics depend strongly on the degree of molecular surface coverage. Atomic force microscope characterization of surfaces exposed to WGA proteins for 1000 s show large protein aggregates consistent with the predicted coverage. These calculations and experiments provide useful insight into the details of molecular motion in confined geometries.

1. Introduction

Protein transport in nanochannels and nanopores is important in separations, microfluidics and in biology [1–9]. Many recent studies have examined the transport of proteins and other molecules near surfaces and in confined geometries [10–21]. For example, lysozyme adsorption to charged surfaces was investigated using Monte Carlo (MC) by Carlsson et al., and it was found that adsorption was favored by high protein concentration and high protein net charge, among other conditions [22]. Ziemys et al. combined experiments and Molecular Dynamics (MD) to study glucose in silica nanochannels. It was observed that the coupling of concentration and confinement effects led to inhibited transport in the nanochannel [23]. The adsorption potential of α-lactalbumin (ALC) and the hen egg white lysozyme (HEWL) on a poly(vinylimidazole) polymer was modeled with classical molecular mechanics calculations at the atomistic level by Noinville et al. Calculations were performed for molecule-surface separations ranging from the bulk to contact, and preferred orientations were identified for the surface-bound proteins as well as effective net charges for the proteins [24]. HEWL adsorption to charged surfaces was also studied by Ravichandran et al. using Brownian Dynamics, and it was determined that the net positively-charged protein can adsorb to a positively-charged surface because of the nature of the charge distribution around the protein molecule [25]. Karnik et al. found that the diffusion of molecules in a nanochannel can strongly depend on the concentration of diffusing molecules in the reservoir [26], which has particular relevance for the present investigation. These studies all provide useful and important insight into molecular transport in confined environments, but they do not fully illuminate the complementary bulk and surface transport mechanisms for individual molecules.

In this work we resolve differences in two molecular transport studies with wheat germ agglutinin (WGA) protein molecules. In the first study, Durand et al. measured diffusion coefficients for fluorescently-labeled wheat germ agglutinin (WGA) in nanochannels, and found an effective diffusion coefficient for confined molecules which is four orders of magnitude lower than its free diffusion coefficient.[27] In the second set of experiments, WGA molecules were observed by fluorescence correlation spectroscopy (FCS) in a nanochannel formed by two parallel borosilicate glass plates separated by 50 nm [28]. The FCS observation volume is well approximated by a right circular cylinder with radius 420 nm. It was found that, depending on the concentration, net charge of the proteins, and the ionic strength of the solution, diffusion was dominated by steric exclusion, the reversible surface adsorption of the biomolecules, or the exclusion-enrichment effect. Under some conditions the effective diffusion coefficient in the

* Corresponding author.
E-mail address: tringe2@llnl.gov (J.W. Tringe).

http://dx.doi.org/10.1016/j.chemphys.2015.04.021
0301-0104/

nanochannel was comparable to the free diffusion coefficient. The number of charges in the nanochannel 'bulk' and on the surface was measured, as well as the bulk diffusion time and the characteristic protein-surface interaction time. As will be demonstrated, our combined MD and MC calculations specifically reflect the motion of molecules in FCS and nanochannel diffusion experiments, and so demonstrate how individual molecules can interact with the surface and the bulk in these confined geometries.

We choose a simple spherical bead to model our protein. Fig. 1 shows the relationship between different degrees of details of protein models used for diffusion studies. Obviously simulations in atomistic details on the necessary length scales of tens of nanometers are impossible. Folded proteins in water are relatively rigid so we can neglect polymeric degrees of freedom. Then the simplest approach is one spherical bead which is matched to the hydrodynamic radius of the overall protein. We are focussing on very large diffusion scales where the protein can be approximated by a single diffusing entity. Clearly such a model cannot explain all the kinetic details of the protein dynamics but it is able to explain the effects to first order. More detailed models as seen in Fig. 1 are being investigated currently (Ustach et al., in preparation).

2. Computational and experimental methods

2.1. Molecular Dynamics

Molecular Dynamics (MD) simulations are performed using a coarse-grained (CG) implicit solvent model. The system is composed of 5000 wall beads interacting with a single protein particle in a cubic simulation box of size $50\sigma \times 52\sigma \times 50\sigma$, where σ is the distance between adjacent beads within a wall. Wall beads are placed at $y = 0.5\sigma$ and $y = 51.5\sigma$ forming two flat surfaces in the x–z plane. The single protein bead is initially positioned at $x = 25\sigma$, $y = 5\sigma$, and $z = 5\sigma$ (cf. Fig. 2).

Simulations are performed with the ESPResSo Molecular Dynamics package [29] in an NVT ensemble. The equations of motions were integrated with the velocity Verlet algorithm using a time step $\delta t = 0.001\ \tau$. To control the temperature and account for hydrodynamic interactions, a dissipative particle dynamics (DPD) thermostat was used. The outcome was compared with the results of the Langevin thermostat, and no significant difference between results from the two thermostats was found. The friction constant was set to $\Gamma = 1.0$ in both cases. Visualization of simulation snapshots was performed with VMD [30].

Non-bonded, short-range interactions between the protein and wall beads are described by a truncated and shifted generalized Lennard-Jones (LJ) potential,

$$U_{LJ}(r) = \left\{ \begin{array}{ll} 4\varepsilon\left[\left(\frac{\sigma}{r}\right)^{2n} - \left(\frac{\sigma}{r}\right)^{n} + c_{shift}\right], & \text{if } r < r_c \\ 0, & \text{if } r \geqslant r_c \end{array} \right\} \quad (1)$$

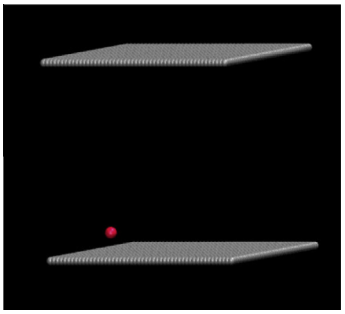

Fig. 2. Initial configuration for MD simulations. A protein bead is simulated in a box of size $50\sigma \times 52\sigma \times 50\sigma$, where σ is the distance between adjacent beads within a wall. The single protein bead is initially positioned at $x = 25\sigma$, $y = 5\sigma$, and $z = 5\sigma$.

where n controls the width of the attraction, ε is the depth of the potential well, σ is the effective minimum distance of approach between two particles, $r_c = 2.5\ \sigma$ is the cut-off radius, and c_{shift} keeps the potential continuous at r_c . The parameters ε, σ, and $\tau = \sigma\sqrt{(m/\varepsilon)}$ (m, bead mass) are chosen as units of energy, length and time, respectively. The diameters of the protein and wall beads are 4σ and σ, respectively. A mapping to real units can be established by selecting σ as 1 nm, which leads to a 4 nm protein diameter. The temperature was chosen as $k_BT = 1.0\varepsilon$. At $T = 298$ K, the thermal energy unit ε is $k_BT = 4.1 \times 10^{-21}\ J \approx 0.6$ kcal/mol. Hence, ε was fixed at 0.6 kcal/mol. Using the known value for the WGA protein mass (38 kDa), τ was found to be 8.08 ns.

Non-bonded, short-range interactions between the protein-wall beads use the (4–2)- and (12–6)-Lennard-Jones potential for systems with no electrostatics and the traditional (12–6)-Lennard-Jones potential for systems with electrostatics. For the system with electrostatics, long-range interactions are modeled by a Debye–Huckel potential as follows:

$$U^{C-DH} = l_B k_B T \frac{q_1 q_2 exp(-\kappa r)}{r} \text{ for } r < r_{cut} \quad (2)$$

where $l_B = e_0^2/(4\pi \in k_BT)$ denotes the Bjerrum length, which measures the strength of the electrostatic interactions; k_B is the Boltzmann constant; T is the temperature; q_1 and q_2 are charges of two interacting particles; r is the separation distance; and κ is the inverse Debye length. As solvent molecules are defined implicitly, l_B is set to 0.7 nm for water at room temperature. The wall (borosilicate glass) surface charge density is -0.64 C/m^2. An ionic strength is set to 10^{-1} M which leads to a Debye length of 0.96 nm. We assume the WGA molecule is positively charged with a charge of +1 at the pH values of interest. Monovalent counterions are introduced to the system to keep overall system charge neutral.

These simulations make it possible to track the motion of an individual protein molecule throughout the $50 \times 52 \times 50$ nm

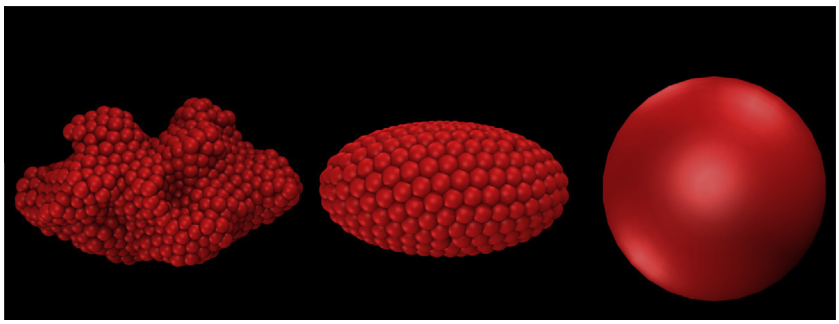

Fig. 1. Different degrees of protein modeling (here BSA) and their relation. The single spherical bead is chosen here.

simulation volume. For the purpose of developing a complete description of the protein path over the much larger FCS observation volume (radius ~420 nm), the single most useful value to be extracted from these simulations is the distance traveled on the surface during one complete surface interaction period, which ends when the molecule transits into the bulk. The mean and standard deviation of the surface distances are calculated as a function of the LJ and Debye–Huckel potential parameters. Production runs are performed for at least 500 μs, and the surface distances are averaged throughout the simulations. The particle visited both surfaces in the simulations with low ε values or stayed closer to one of the surfaces otherwise. Hence, to ensure particle surface interactions throughout the simulations the particle is initially placed close to one of the surfaces. The initial position of the particle in x–z plane, however, does not affect the mean distance results as periodic boundary condition is applied.

2.2. Monte Carlo

The Monte Carlo simulation code is implemented in Mathematica, and takes as inputs two assumed Gaussian step size distributions, surface and bulk, with associated time distributions. The surface step size distribution is obtained directly from the MD calculations as previously described. The bulk mean step size, r, is the bulk diffusion distance defined from:

$$r = \sqrt{(6 D_{bulk} \tau_{bulk})} \tag{3}$$

where τ_{bulk} is the bulk diffusion time (6×10^{-4} s for WGA in calculations to follow), and D_{bulk} is the bulk diffusion coefficient. It assumed that the standard deviation of the r distribution is one fifth of r.

For each system, a constant parameter P_{surf} is defined to reflect the probability that a molecule is on the surface at any given step in the Monte Carlo simulation. P_{surf} accounts for the effects of the electrical double layer (EDL) and surface history (surface protein concentration) as will be discussed.

We also introduce a distribution t_{surf} to reflect the time of interaction of the protein molecules with the surface. This distribution is determined in part by f_{surf}, the fraction of the surface covered by WGA molecules. t_{surf} is also characterized by t_{sb} and t_{sc}, which are the average times a protein molecule could spend on a bare surface and a protein-covered surface, respectively. Below we use $t_{sb} = 10\ \tau_{bulk}$, and $t_{sc} = \tau_{bulk}/10$. Specifically, we assume a bimodal distribution for t_{surf}, using normal distributions with mean values t_{sb} and t_{sc}. The two normal distributions are weighted using f_{surf} for t_{sc} and $(1-f_{surf})$ for t_{sb}. The standard deviations of the two modes are assumed to be one fifth of the averages, as shown in Fig. 3.

The MC simulation follows a set of molecules from a common origin through the step that takes each molecule across the boundary of the FCS observation volume. FCS measurements are sensitive only to transitions of molecules across the observation volume boundary, so these statistics are the most relevant for comparison to experiment. The number of steps and total transit time along the path from origin to boundary are calculated for each molecule in MC.

At every MC step, the molecule is probabilistically determined based on a constant P_{surf} to be either on the surface or in the bulk. For a given configuration P_{surf} takes into account the presence of the electrical double layer by taking low values when the EDL thickness is an appreciable fraction of the nanochannel height. Next, three quantities are calculated: the molecule travel direction, the molecule travel distance, and the molecule travel (or residence) time. First, the molecule travel direction is determined. Although molecules are confined to a very narrow channel in the bulk, their three dimensional motions must be taken into account. This is accomplished by defining the travel direction using two angles. An angle in the x–z plane parallel to the nanochannel walls is randomly chosen between 0 and 2π. The orthogonal angle measured from the y-axis is randomly chosen between 0 and π. If a molecule is on the surface, only the angle in the x–z plane is used for the travel direction. Next, the molecule travel distance is calculated. If the molecule is on the surface, the travel distance is determined from the distribution determined using MD as previously noted. If the molecule is in the bulk, the travel distance is determined from a Gaussian distribution with mean equal to the bulk step size, assuming that the molecule is initially centered in the y direction between the nanochannel walls. If the travel direction is defined such that the molecule would impinge on a nanochannel wall the bulk travel distance is truncated at the point of intersection. The channel height available for bulk molecular transport is reduced by $2\lambda_D$ to account for the Debye screening length [28]:

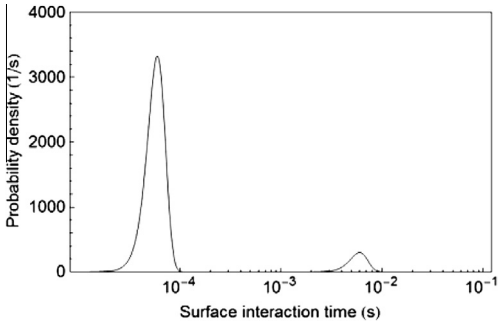

Fig. 3. Bimodal probability function for surface interaction time, t_{surf}. t_{surf} is characterized by $t_{sb,}$ the average time a protein spends on a bare surface, and t_{sc}, the average time a protein spends on a protein-covered surface. We assume a bimodal distribution for t_{surf}, using normal distributions with mean values $t_{sb} = 10\ \tau_{bulk}$ and $t_{sc} = \tau_{bulk}/10$. The two normal distributions are weighted using f_{surf} for t_{sc} and $(1 - f_{surf})$ for t_{sb}. Here $f_{surf} = 0.25$.

$$\lambda_D = \sqrt{\frac{\varepsilon_0 \varepsilon_r RT}{2F^2 c_i}} \tag{4}$$

where ε_0 is the dielectric constant in vacuum, ε_r is the relative permittivity, R is the molar gas constant, F is the Faraday constant and c_i is the ionic strength of the solution.

Finally, the molecule travel or residence time is calculated. If the molecule is on the surface, then the surface interaction time is determined from the t_{surf} distribution previously discussed. If the molecule is in the bulk, then the bulk transit time is taken from the Gaussian distribution with mean value τ_{bulk}, the bulk diffusion time, scaled by ratio of the actual (usually truncated) travel distance to the bulk diffusion distance.

These calculations are repeated until the molecule crosses the circular FCS volume boundary; the total number of steps and the total transit time is stored. Then the same calculations are performed for every other molecule in the set. Although the calculation geometry matches the FCS experimental configuration, it is also appropriate for calculation of an effective diffusion coefficient, which can be compared to coefficients extracted from any other nanochannel experiment.

2.3. Atomic force microscopy

WGA proteins were imaged by atomic force microscopy (AFM) on glass surfaces at concentrations and times that are representative of conditions under which FCS experiments were performed. For example, AFM images were obtained from a clean silicon dioxide surface (control), and from two surfaces which had been incubated for 1000 s with WGA at 50 nM concentration. AFM imaging was performed in air after the surfaces were well-rinsed with DI water and dried with flowing air. Although these images are not directly representative of the *in situ* protein surface concentration under liquid,

they do provide useful information on the degree of protein coverage that is present. The protein concentration on the dried surfaces is likely a conservative lower bound for the concentration present under liquid, given the rinsing performed on the samples prior to imaging which would remove lightly-bound proteins.

3. Results

3.1. Molecular Dynamics

From the ESPResSo MD calculations, the surface step distance is calculated for WGA molecules by averaging the mean distances traveled during each time slot when the molecule makes consecutive steps on the wall. These values are determined for a range of LJ well depths and widths, with and without electrostatic forces, as shown in Table 1.

3.2. Monte Carlo

Using the MC model, we calculate the number of steps and the total transit times for molecules with well depth 1.0, $n = 6$, with electrostatics. Artifacts associated with early exit of the particle from the FCS interaction volume are avoided by assuming the particle is initially centered in the cylindrical volume with height 50 nm and radius 420 nm (dimensions matching the experimental configuration reported in Durand [28]). The effect of moving the particle toward the observation volume edge will be systematically examined later in this paper.

Typical simulation results for number of steps and average route time are shown in Fig. 4(a) and (b), respectively. Fig. 4(c) schematically shows the molecular paths for simulations with 20 and 1000 molecules, superimposed on the outline of the circular FCS observation volume. Simulation results for 20 molecules are shown for clarity, so that the paths of individual molecules may be more easily visualized.

Key variables are summarized in Table 2 for an ensemble of MC simulations with parameters chosen to match previously-reported experimental conditions [27,28].

In Table 3 we summarize MC-calculated effective diffusion values and related parameters, together with experimental parameters from two complementary experimental studies. In the first, Durand 2007 [27], fluorescently-labeled WGA protein molecules were observed with an imaging system to transit nanochannels, and an effective diffusion coefficient $\sim 10^4$ smaller than the bulk diffusion coefficient was inferred. In a second study, [28], fluorescent correlation spectroscopy (FCS) was employed to establish the effective diffusion coefficient for WGA under a range of different ionic concentrations. In this second study, diffusion coefficients similar to the bulk coefficient were observed under some conditions, but smaller values were also measured. A hypothesis was presented to explain the observed differences based on interactions of the WGA molecules with the nanochannel surfaces and with the electrical double layer.

In Table 3 we also calculate a number of surface molecules, N_{surf}, assuming molecules with a hydrodynamic radius r_{WGA} of 3 nm cover a fraction f_{surf} of the circular top and bottom of the cylinder. In other words,

$$N_{surf} = \frac{2 f_{surf} A_{FCS}}{A_{WGA}} \tag{5}$$

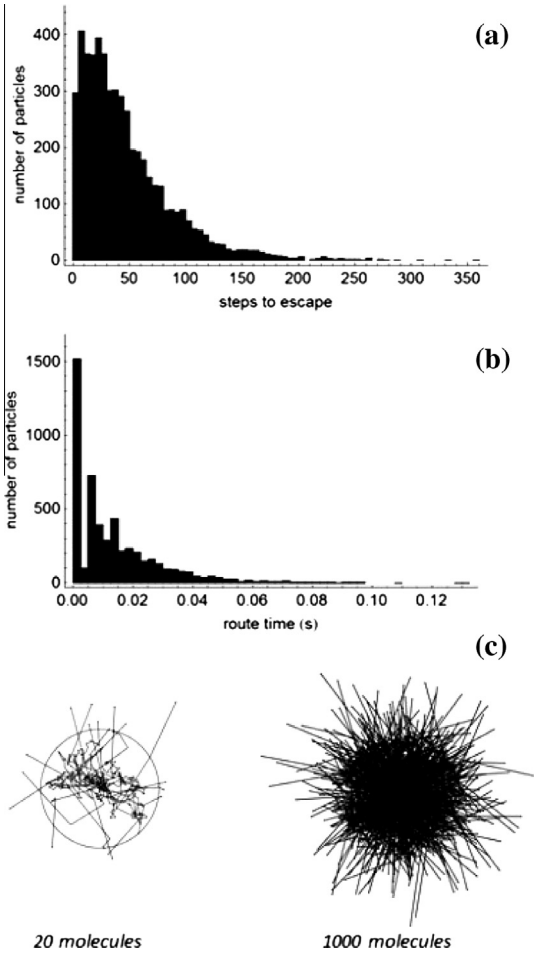

Fig. 4. (a) Number of steps to cross boundary, average = 32 (b) route time, average = 0.008 s (c) path schematic for 20 and 1000 molecules. t_{surf}. $c_i = 9.2 \times 10^{-4}$ M, $c_{WGA} = 50$ nM; $f_{surf} = 0.25$; $N_{surf} = 7.8 \times 10^3$; $N_{surf}/N_{bulk} = 4.0 \times 10^4$; $f_{ch} = 0.59$; $P_{surf} = 0.05$.

where A_{FCS} is the area of the circular top and bottom of the cylinder ($=\pi * (420\ \text{nm})^2$) and $A_{WGA} = \pi * r_{WGA}{}^2$. For all simulations we assume a molar concentration c_{WGA} of 50 nM, and surface transport distance 10.3 ± 9.4 from the MD from the $\varepsilon = 1$, $n = 2$ scenario. However, choosing different surface transport distances from among those simulated does not qualitatively change the results in Table 3, as demonstrated in Table 4.

When the surface probability is high (e.g., 0.99 for the pristine nanochannel case), 30% of the particles "stagnated" or did not exit the cylindrical volume with radius 420 nm in the maximum 500 steps allowed. The time is only calculated for particles which exit the volume, but the effective diffusion constant D_{nc} is calculated for all particles independent of whether they exit the volume. In general, simulations summarized in Table 3 systematically probe the effect of surface coverage (through f_{surf}) and probability of surface interaction (through P_{surf}) on the time proteins spend in the nanochannel (t_{route}) which can then be compared to experimental values.

Table 1
Surface transport distances from MD simulations.

Energy Depth, ε	0.1, $n = 2$ no electrostatics	1.0, $n = 2$ no electrostatics	0.1, $n = 6$ no electrostatics	1.0, $n = 6$ no electrostatics	1.0, $n = 6$ with electrostatics
Distance, nm	10.3 ± 9.4	36.6 ± 36.8	13.5 ± 25.4	12.7 ± 18.2	5.9 ± 4.5

Table 2
Variables for MC simulations.

c_i	Ionic concentration (M)
f_{surf}	Fraction of the surface assumed covered with proteins
N_{surf}	Number of proteins implied by the fractional coverage
N_{surf}/N_{bulk}	Ratio of proteins on surface to proteins in bulk, assuming 50 nM protein concentration in bulk, and channel height reduced by EDL
f_{ch}	Fraction of the total channel height h available for bulk particles, assuming channel is reduced by twice the Debye screening length
P_{surf}	Assumed probability that a protein will interact with the surface, determined by the thickness of the EDL and protein surface concentration
t_{route}	Median time for protein to move from the center of the cylindrical volume to the edge, 420 nm from the center (s)
D_{nc}	The effective diffusion constant in the nanochannel

For the MC simulations matched to conditions in the Durand 2009 experiment, D_{bulk}/D_{nc} is shown in a bar chart in Fig. 5. The route time values are higher but on the same order of magnitude as the FCS-extracted diffusion times at these ionic concentrations.

For the Durand 2007 experiment the evaluated diffusion constant is the same order of magnitude as the experimentally-measured value, ~10,000 times higher than the bulk diffusion constant. These results show that the qualitative behavior in both the FCS [28] and nanochannel [27] experiments can be matched with appropriate selections of the fractional surface coverage of proteins, f_{surf}, and the probability of surface interaction P_{surf} which are both physically plausible and internally consistent.

The effect of modifying the surface step size (as calculated by MD) on the mean number of steps to cross the boundary, and the time taken, is shown in Table 4 for 1000-molecule MC simulations. Note that since these step size values are all small relative to the radius of the FCS cylinder, the overall effect of changing the surface step size on the average time it takes for a molecule to cross the FCS observation boundary is limited. For example, the median time ranges from 9 ms in the case of an energy depth ε of 1 eV ($n = 2$), no electrostatics, to 16 ms for the case with $\varepsilon = 1$ eV ($n = 6$), with electrostatics. To generate values shown in Table 4 we assumed $c_i = 0.36$ M, $c_{WGA} = 50$ nM, $f_{surf} = 0.95$, $N_{surf} = 3.7 \times 10^4$, $f_{ch} = 0.98$ and $P_{surf} = 0.75$. Simulations with electrostatics are assumed to be most comparable to experimental conditions.

Finally, we use the MC model examine the effect of moving the initial position of the molecule away from the center of the cylindrical observation volume. Fig. 6 shows the average number of steps and average time for a molecule to cross the observation volume boundary as a function of initial position of the molecule. The position is scaled by the observation volume radius. Simulations are performed for 1000 molecules, where each molecule is tracked for up to 500 steps. Almost all molecules initially inside the volume ($y/r < 1$) cross the boundary in many fewer than 500 steps. Molecules initially outside the volume may or may not cross, however. The mean times and steps reported for $y/r > 1$ are calculated only for those particles which cross, by definition.

The total number of boundary crossing molecules is also shown in Fig. 6 as a function of initial position. When the molecule starts its travel one radius away from the observation volume edge, only about of the molecules eventually cross the boundary. To generate the initial position data shown in Fig. 6, we assume $c_i = 0.36$ M, $c_{WGA} = 50$ nM, $f_{surf} = 0.95$, $N_{surf} = 3.7 \times 10^4$, $f_{ch} = 0.98$ and $P_{surf} = 0.75$.

3.3. Atomic force microscopy (AFM)

Because our model assumes high concentrations of WGA proteins on the surface, we use atomic force microscopy (AFM) to

Table 3
Monte Carlo results (1000 particle simulations) for parameters reflecting experimental parameters [27,28]; $D_{bulk} = 7.6 \times 10^{-11}$ m^2/s.

Ref.	c_i [M]	f_{surf}	N_{surf}	N_{surf}/N_{bulk}	f_{ch}	P_{surf}	D_{nc} (m^2/s) mean (standard deviation), median	t_{route} (s) mean (standard deviation), median	t_{route} (s) (exp)
[28]	4.1×10^{-4}	0.10	3.9×10^3	1.2×10^4	0.39	0.01	3.8×10^{-10} (5.0×10^{-9}) 3.1×10^{-11}	3.9×10^{-3} (5.5×10^{-3}) 1.2×10^{-3}	10^{-2}
[28]	4.1×10^{-4}	0.10	3.9×10^3	1.2×10^4	0.39	0.05	1.8×10^{-10} (1.3×10^{-9}) **4.3×10^{-12}**	1.4×10^{-2} (1.5×10^{-2}) **1.0×10^{-2}**	
[28]	4.1×10^{-4}	0.10	3.9×10^3	1.2×10^4	0.39	0.10	5.1×10^{-10} (1.1×10^{-8}) 2.2×10^{-12}	2.8×10^{-2} (2.7×10^{-2}) 2.1×10^{-2}	
[28]	3.6×10^{-1}	0.95	3.7×10^4	4.6×10^4	0.98	0.90	9.8×10^{-12} (5.6×10^{-11}) 1.0×10^{-12}	5.4×10^{-2} (4.8×10^{-2}) 4.2×10^{-2}	10^{-2}
[28]	3.6×10^{-1}	0.95	3.7×10^4	4.6×10^4	0.98	0.65	3.4×10^{-11} (1.3×10^{-10}) **4.7×10^{-12}**	1.4×10^{-2} (1.4×10^{-2}) **9.3×10^{-2}**	
[28]	3.6×10^{-1}	0.95	3.7×10^4	4.6×10^4	0.98	0.40	2.4×10^{-10} (5.0×10^{-9}) 1.9×10^{-11}	5.0×10^{-3} (6.4×10^{-3}) 1.9×10^{-3}	
[28]	9.2×10^{-4}	0.25	9.8×10^3	2.0×10^4	0.59	.05	3.4×10^{-10} (3.1×10^{-9}) 7.8×10^{-12}	8.5×10^{-3} (9.9×10^{-3}) 6.3×10^{-3}	2×10^{-3}
[28]	9.2×10^{-4}	0.25	9.8×10^3	2.0×10^4	0.59	.03	6.6×10^{-10} (1.1×10^{-8}) **2.0×10^{-11}**	5.9×10^{-3} (7.4×10^{-3}) **1.8×10^{-3}**	
[28]	9.2×10^{-4}	0.25	9.8×10^3	2.0×10^4	0.59	0	3.1×10^{-10} (1.9×10^{-9}) 5.4×10^{-11}	1.0×10^{-3} (9.3×10^{-4}) 8.3×10^{-4}	
[27]	4.1×10^{-4}	10^{-3}	39	120	0.39	0.99	1.7×10^{-14} (9.1×10^{-14}) 8.4×10^{-15}	3.1 (1.4) 3.1	N/A
[27]	4.1×10^{-4}	10^{-4}	4	12	0.39	0.99	1.9×10^{-14} (2.0×10^{-13}) **8.0×10^{-15}**	3.1 (1.4) **3.0**	

Table 4
The effect of modifying the surface on the mean number of steps to cross the boundary and the time taken to cross the boundary (1000 molecule MC simulations).

Energy depth, ε	0.1, $n = 2$ no electrostatics	1.0, $n = 2$ no electrostatics	0.1, $n = 6$ no electrostatics	1.0, $n = 6$ no electrostatics	1.0, $n = 6$ with electrostatics
Distance (nm)	10.3 ± 9.4	36.6 ± 36.8	13.5 ± 25.4	12.7 ± 18.2	5.9 ± 4.5
Number of steps: mean (standard deviation), median	73 (60), 58	46 (36), 37	62 (50), 51	65 (52), 54	75 (64), 58
Time (ms): mean (standard deviation), median	20 (20), 15	13 (13), 9	17 (17), 13	18 (18), 14	21 (21), 16

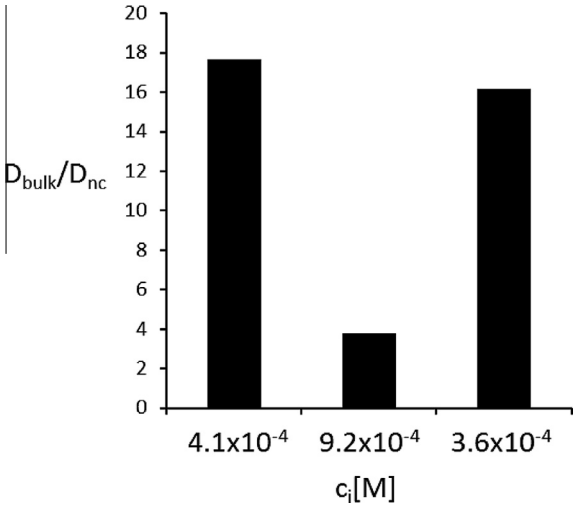

Fig. 5. The ratio of the bulk diffusion constant to the MC-calculated diffusion constant in the nanochannel for three ionic concentrations which are the same as have been experimentally measured in Durand et al., 2009 [28].

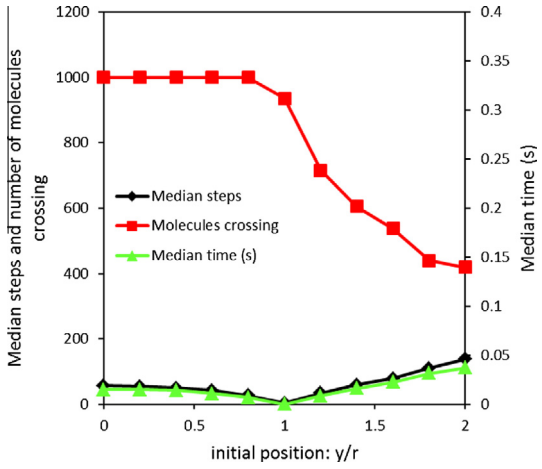

Fig. 6. Mean number of steps, mean time for a molecule to cross the cylindrical observation volume boundary, and number of molecules (out of 1000) crossing the boundary, as a function of the initial position of the molecule. The position is scaled by the observation volume radius. Each molecule is tracked for up to 500 steps.

experimentally support our hypothesis that WGA proteins do in fact bind strongly to silicon oxide surfaces. Fig. 7 shows thresholded, flattened AFM images of a clean silicon dioxide surface, and of two surfaces which have been incubated for 1000 s with WGA at 50 nM concentration. As noted previously, AFM imaging was performed in air after the surfaces were well-rinsed with DI water and dried with flowing air. Fig. 7(a) is the surface which was incubated with 50 nM WGA in 1 mM PBS (pH 7), and Fig. 7(b) is the surface which was incubated with 50 nM WGA in 100 mM PBS (pH 7).

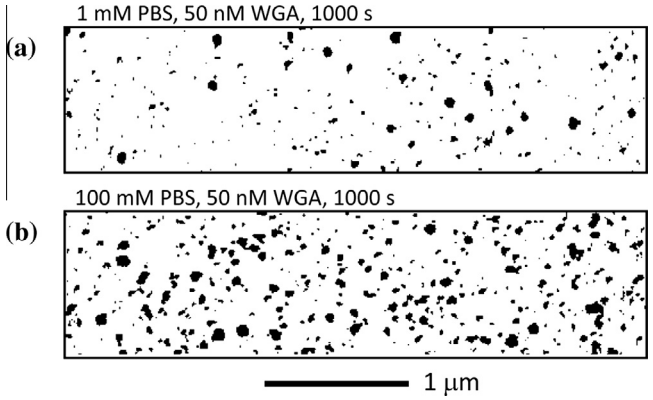

Fig. 7. (a) Surface incubated with 50 nM WGA in 1 mM PBS (pH 7) for 1000 s, then rinsed with DI water and dried (b) surface incubated with 50 nM WGA in 100 mM PBS (pH 7) for 1000 s, then rinsed with DI water and dried.

Table 5 summarizes the particle size statistics for the images shown in Fig. 7, together with statistics from a control sample.

4. Discussion

Fig. 7 and Table 5 demonstrate that there is a significant degree of WGA protein adsorption on SiO_2 surfaces after 1000 s at both 1 and 100 mM PBS concentrations. These values can be taken as lower bounds on the density of WGA molecules on surfaces at times comparable to those used in FCS experiments. However, the proteins appear not affected by surface charges in the same way as proteins in nanochannels, where FCS results suggest greater surface interactions would be observed for the 1 mM PBS solutions [28]. This may be because on these open surfaces, unlike in nanochannels, molecules are not as excluded from approaching the surface due to overlapping electrical double layers. In any case, the observation of bound proteins on these surfaces in such significant concentrations for both 1 and 100 mM PBS concentrations complements and qualitatively supports the results obtained by FCS, where it was inferred that the number of molecules on the surface exceeded the number in the bulk, and that the time a given molecule spends on the surface exceeds the time spent in the bulk. In effect, the presence of the WGA molecules observed by AFM is independent experimental confirmation of a robust attractive protein-surface interaction.

Karnik et al. have presented compelling evidence that suggests the diffusion in a nanochannel can be controlled by the concentration of the diffusing species in the reservoir, under the conditions when the diffusing molecules bind to the nanochannel surfaces [26]. The study investigated of streptavidin in biotin-functionalized nanofluidic channels. Under these surface-binding conditions the ratio of the bulk constant D_{bulk} to the effective diffusion constant in the nanochannel, D_{eff} is given by:

$$\frac{D_{bulk}}{D_{eff}} = \frac{\gamma_0}{hc} \tag{6}$$

Table 5
Particle size analysis for WGA on silicon dioxide surface, with control surface (4 × 1 um).

Surface	Number of particles	Mean particle height (nm)	Sigma height(nm)	Mean particle diameter (nm)	Sigma diameter(nm)
Clean SiO_2	13	3.23	0.07	9.59	1.90
50 nM WGA, 1 mM PBS	245	4.72	2.19	22.5	15.3
50 nM WGA, 100 mM PBS	406	5.52	2.47	31.5	20.3

Note that the 'particles' in Table 5 do not represent individual proteins since their mean diameters are much larger than the ~3 nm hydrodynamic radius of WGA proteins and the ~10 nm diameter of the AFM tip. Instead, each particle represents a WGA protein aggregate.

where h is the nanochannel height, c the reservoir concentration and γ_0 the molecular binding density at the surface. From Durand et al. [27], $D_{bulk}/D_{eff} = 10^4$ and h is 50 nm, then for $c_{WGA} = 3 \times 10^{19}\ m^{-3}$ the implied binding density is $\sim 10^{16}\ m^{-2}$. For the FCS area $\sim 10^{-12}\ m^2$ this suggests a total number of surface molecules N_{surf} on the order of 10^4, which is the order of magnitude estimated in Table 3 for nanochannel surfaces exposed to WGA molecules before the FCS measurements are made [28].

From Table 1, MD indicates that the well depth and width both affect the surface transit path, but in different ways. For a well width corresponding to a modified LJ potential with $n = 2$, increasing the well depth by an order of magnitude from 0.1 to 1 ε has a significant effect on the path length, increasing the average length by more than a factor of 3, from 10.3 to 36.6 nm. For a narrower well width corresponding to the classical LJ potential with $n = 6$, however, increasing the well depth over the same 0.1 to 1 ε range hardly changes the average path length: in both cases the length is near 13 nm. Note that in all cases there is considerable variability in the distances by different molecules, such that the standard deviation is equal or even greater than the mean. For the well width corresponding to $n = 6$, the variability is especially pronounced, with the standard deviation being 1.5–2 times the mean.

Adding electrostatic forces by the Debye–Huckel potential has the effect of significantly decreasing the average path length, to 5.9 nm. The standard deviation (4.5 nm) is again a large fraction of the average. Because of the presence of surface and molecular charges in the nanochannel, it is likely that that this combined LJ–Debye Huckel potential best reflects the physical system tested by FCS in Durand et al. To illustrate particle paths with the Monte Carlo model in Fig. 4, we therefore use MD values from the combined LJ-Debye Huckel potential with assumptions described in Table 3. Both the average number of steps to cross the FCS observation volume boundary and the total time within the boundary have monomodal distributions with relatively long tails. The average number of steps is 158, and the average time is 52 ms. Note from Fig. 4(c) that the molecular transport is actually dominated by diffusion paths in the channel bulk, with molecular motion highly localized when on the surface. This behavior is a direct consequence of the fact that the bulk molecular transport distance is about 100 times larger than the average transport distance as estimated by MD.

Table 4 also shows the effect of modifying the surface potential on the number of steps and time spent in the observation volume. It is interesting to note that these quantities closely reflect the surface step distances, although processes in the bulk dominate the molecular transport across the full volume. The total steps and time are similar for $\varepsilon = 0.1$, $n = 2$ without electrostatics, and $\varepsilon = 1$, $n = 6$, with electrostatics. Since the computation time is much greater with electrostatics, this similarity may indicate a possible path toward improved computational efficiency for conditions when the surface step mean and standard deviation are comparable, and when both are much smaller than the mean bulk step after validation.

An important result from the Monte Carlo model-derived values in Table 3 and Fig. 5 is the quantitative description of surface characteristics that are most effective for determining the transport rate of molecules in nanochannels. Consistent with the results of Karnik et al., the probability of a molecule's interaction with the surface, P_{surf}, is the single most important parameter, but this probability is in turn determined by fraction of the channel not excluded by the EDL, f_{ch}. The time the molecules spend on the surface is affected by the fraction of the surface covered by molecules, f_{surf} through the bimodal distribution shown in Fig. 3. Taken together, P_{surf}, f_{ch} and f_{surf} effectively determine the rate at which molecules transit a confined volume such as a nanochannel.

Finally, Fig. 6 shows the effect of the molecule's initial position within an observation volume. These results are helpful for understanding the FCS experiment since the molecular position is not directly observable. Monte Carlo results show that for the large majority of initial positions, the total number of steps and time spent within the observation volume are comparable to one another. Only when the molecule is very near the edge does the number of steps and time begin to drop significantly. Furthermore, molecules initially outside the volume are unlikely to affect the total step and time values, since molecules just half a radius away from the edge take a relatively long time to reach the boundary. The step times and number of steps shown in Fig. 6 for molecules initially outside the FCS observation volume ($y/r > 1$) are actually a lower bound, since the molecules which take more than 500 steps without crossing the boundary are not included.

4.1. Conclusions

We report on modeling of molecular interactions with surfaces relevant for understanding WGA protein transport in nanochannels. An important result of the combined MC and Molecular Dynamics simulations is an estimation of the total time and distance traveled by single WGA molecules transiting nanochannels observed by FCS and by optical microscopy [27,28]. This work presents a hypothesis to explain the large differences in observed diffusion coefficients in these two experimental conditions by quantitatively estimating the probability and time of interaction of WGA molecules with surfaces. Our calculations indicate that the small diffusion coefficients estimated from optical microscopy in nanochannels are likely a result of surface binding of WGA molecules with the nanochannel, consistent with previous observations of streptavidin in biotin-functionalized nanofluidic channels [26]. Relative to the nanochannels observed by optical microcrosopy, our model suggests higher WGA surface concentrations in the nanochannels observed by FCS where proteins are present in solution for significant times before the FCS measurements are made. This conclusion is supported by AFM measurements on glass surfaces exposed to WGA proteins for 1000 s, where aggregates of WGA are consistently observed. For FCS measurements, the variation in the effective diffusion times then likely results from the EDL lowering the probability of surface interaction, and from the longer times that molecules spend on surface with lower protein surface coverage.

We employed MD to estimate the surface transport distance and also the importance of the interaction potential for neutral molecules, compared the electrostatic potential between a charged protein molecule and the glass surface. For a potential which includes both the nonbonded short range interactions

reflected by the LJ potential, as well as electrostatic interactions reflected by the Debye Huckel potential, the surface path length is about 5.9 ± 4.5 nm. This value is at least half the value of surface path length when electrostatic effects are neglected. The Monte Carlo model with MD input estimates the paths of protein molecules on surfaces and in the 'bulk' regime near surfaces. For the case when both the non-bonded short range interactions and electrostatic interactions are accounted for, the average number of steps for a molecule in the ~420 nm radius FCS interrogation volume is 158, and the average time spent in the volume is 52 ms. In general, the average number of steps and time spent in the volume reflect the surface step distances determined by the molecule-surface interaction potential, though the probability of surface interaction and the time spent at the surface are also very important for establishing transport characteristics of WGA protein molecules in nanochannels.

Conflict of interest

We have no conflicts of interest in this paper.

Acknowledgements

This work was supported by a Grant from the University of California Office of the President UCOP Lab Fee Program (Grant Number 12-LR-237353). One of us, Nazar Ileri, acknowledges the support of the U.S. National Science Foundation I2CAM International Materials Institute Award, Grant DMR-0844115. We are grateful for helpful discussions with Dr. Christine Orme at LLNL and Dr. Paul Ashby at Lawrence Berkeley National Lab regarding protein imaging with AFM. This work was partially performed under the auspices of the U. S. Department of Energy by Lawrence Livermore National Laboratory under Contract DE-AC52-07NA27344.

Appendix

A sensitivity study was performed to examine the effect of changing parameters applied in the Monte Carlo model: f_{surf}, the fraction of the surface covered by WGA molecules, f_{ch}, (the fraction of the total channel height available for bulk particles, assuming channel is reduced by twice the Debye screening length), and t_{sb} and t_{sc}, (the average times a protein molecule could spend on a bare surface and a protein-covered surface, respectively). In general parameter values were selected based on the physical properties of the nanochannel under tested conditions, but it is illuminating to further examine these roles these values play in determining the effective diffusion coefficient and route time, since these can be compared with experimentally-measured values.

c_i [M]	f_{surf}	t_{sb}, t_{sc}	f_{ch}	P_{surf}	D_{nc} (m^2/s) mean (standard deviation), median	t_{route} (s) mean (standard deviation), median	t_{route} (s) (exp)
4.1×10^{-4}	**0.01**	$\tau_{bulk} * 10$, $\tau_{bulk}/10$	0.39	0.05	1.3×10^{-10} (6.3×10^{-10}) 4.0×10^{-12}	1.6×10^{-2} (1.7×10^{-2}) 1.3×10^{-2}	10^{-2}
4.1×10^{-4}	**0.05**	$\tau_{bulk} * 10$, $\tau_{bulk}/10$	0.39	0.05	1.3×10^{-10} (7.7×10^{-10}) 4.3×10^{-12}	1.5×10^{-2} (1.6×10^{-2}) 1.0×10^{-2}	
4.1×10^{-4}Reference	**0.1**	$\tau_{bulk} * 10$, $\tau_{bulk}/10$	0.39	0.05	1.8×10^{-10} (1.3×10^{-9}) **4.1×10^{-12}**	1.5×10^{-2} (1.5×10^{-2}) **1.2×10^{-2}**	
4.1×10^{-4}	**0.5**	$\tau_{bulk} * 10$, $\tau_{bulk}/10$	0.39	0.05	1.8×10^{-10} (1.6×10^{-9}) 8.4×10^{-12}	8.1×10^{-3} (9.8×10^{-3}) 6.3×10^{-3}	
4.1×10^{-4}	0.1	$\tau_{bulk} * 10$, $\tau_{bulk}/10$	**0.2**	0.05	3.4×10^{-10} (3.3×10^{-9}) 2.4×10^{-12}	2.7×10^{-2} (2.5×10^{-2}) 2.0×10^{-2}	10^{-2}
4.1×10^{-4} Reference	0.1	$\tau_{bulk} * 10$, $\tau_{bulk}/10$	**0.39**	0.05	1.8×10^{-10} (1.3×10^{-9}) **4.1×10^{-12}**	1.5×10^{-2} (1.5×10^{-2}) **1.2×10^{-2}**	
4.1×10^{-4}	0.1	$\tau_{bulk} * 10$, $\tau_{bulk}/10$	**0.8**	0.05	2.4×10^{-10} (1.5×10^{-9}) 9.6×10^{-12}	7.6×10^{-3} (9.7×10^{-3}) 5.6×10^{-3}	
9.2×10^{-4}	0.1	**$\tau_{bulk} * 5$,** $\tau_{bulk}/10$	0.39	0.05	3.0×10^{-10} (3.2×10^{-9}) 8.8×10^{-12}	7.6×10^{-3} (7.9×10^{-3}) 5.3×10^{-3}	10^{-2}
9.2×10^{-4} Reference	0.1	**$\tau_{bulk} * 10$,** $\tau_{bulk}/10$	0.39	0.05	1.8×10^{-10} (1.3×10^{-9}) **4.1×10^{-12}**	1.5×10^{-2} (1.5×10^{-2}) **1.2×10^{-2}**	
9.2×10^{-4}	0.1	**$\tau_{bulk} * 20$**, $\tau_{bulk}/10$	0.39	0.05	1.2×10^{-10} (7.3×10^{-10}) 2.4×10^{-12}	2.8×10^{-2} (2.8×10^{-2}) 2.0×10^{-2}	
4.1×10^{-4}	0.1	$\tau_{bulk} * 10$, **$\tau_{bulk}/5$**	0.39	0.05	3.7×10^{-10} (4.8×10^{-9}) **4.4×10^{-12}**	1.5×10^{-2} (1.6×10^{-2}) **1.1×10^{-2}**	10^{-2}
4.1×10^{-4} Reference	0.1	$\tau_{bulk} * 10$, **$\tau_{bulk}/10$**	0.39	0.05	1.8×10^{-10} (1.3×10^{-9}) **4.1×10^{-12}**	1.5×10^{-2} (1.5×10^{-2}) **1.2×10^{-2}**	
4.1×10^{-4}	0.1	$\tau_{bulk} * 10$, **$\tau_{bulk}/20$**	0.39	0.05	2.2×10^{-10} (1.4×10^{-9}) **4.3×10^{-12}**	1.5×10^{-2} (1.6×10^{-2}) **1.1×10^{-2}**	

References

[1] Z. Siwy, E. Heins, C.C. Harrell, P. Kohli, C.R. Martin, J. Am. Chem. Soc. 126 (2004) 10850.
[2] Z. Siwy, L. Trofin, P. Kohli, L.A. Baker, C. Trautmann, C.R. Martin, J. Am. Chem. Soc. 127 (2005) 5000.
[3] N. Ileri, R. Faller, A. Palazoglu, S.E. Letant, J.W. Tringe, P. Stroeve, Phys. Chem. Chem. Phys. 15 (2013) 965.
[4] N. Ileri, S.E. Letant, A. Palazoglu, P. Stroeve, J.W. Tringe, R. Faller, Phys. Chem. Chem. Phys. 14 (2012) 15066.
[5] N. Ileri, P. Stroeve, A. Palazoglu, R. Faller, S.H. Zaidi, H.T. Nguyen, J.A. Britten, S.E. Letant, J.W. Tringe, J. Micro-Nanolithogr, Mems Moems 11 (2012).
[6] R.B. Schoch, A. Bertsch, P. Renaud, Nano Lett. 6 (2006) 543.
[7] R.B. Schoch, J. Han, P. Renaud, Rev. Mod. Phys. 80 (2008) 839.
[8] M. Barsbay, O. Guven, H. Bessbousse, T.L. Wade, F. Beuneu, M.-C. Clochard, J. Membr. Sci. 445 (2013) 135.
[9] L. Yue, L. Ping, X. Li, F. Dingyan, H. Shasheng, J. Membr. Sci. 453 (2014) 12.
[10] H.-L. Gao, C.-Y. Li, F.-X. Ma, K. Wang, J.-J. Xu, H.-Y. Chen, X.-H. Xia, Phys. Chem. Chem. Phys. 14 (2012) 9460.
[11] G. Hong-Li, L. Cheng-Yong, M. Feng-Xiang, W. Kang, X. Jing-Juan, C. Hong-Yuan, X. Xing-Hua, Phys. Chem. Chem. Phys. 14 (2012) 9460.
[12] A. Mani, T.A. Zangle, J.G. Santiago, Langmuir 25 (2009) 3898.
[13] D. Huh, K.L. Mills, X. Zhu, M.A. Burns, M.D. Thouless, S. Takayama, Nat. Mater. 6 (2007) 424.
[14] R. Karnik, K. Castelino, R. Fan, P. Yang, A. Majumdar, Nano Lett. 5 (2005) 1638.
[15] S.J. Kim, Y.-C. Wang, J.H. Lee, H. Jang, J. Han, Phys. Rev. Lett. 99 (2007).
[16] S.M. Kim, M.A. Burns, E.F. Hasselbrink, Anal. Chem. 78 (2006) 4779.
[17] W.H. Fissell, A. Dubnisheva, A.N. Eldridge, A.J. Fleischman, A.L. Zydney, S. Roy, J. Membr. Sci. 326 (2009) 58.
[18] M. Jian-Qiang, Y. Tao, C.J. Kurth, S. Qiang, Z. Yu-Feng, J. Membr. Sci. 401–402 (2012) 109.
[19] K. Malek, R.A. van Santen, J. Membr. Sci. 311 (2008) 192.
[20] M. Pourali, A. Maghari, Chem. Phys. 444 (2014) 30.
[21] R. Hannaoui, G. Galliero, D. Ameur, C. Boned, Chem. Phys. 389 (2011) 53.
[22] F. Carlsson, E. Hyltner, T. Arnebrant, M. Malmsten, P. Linse, J. Phys. Chem. B 108 (2004) 9871.
[23] A. Ziemys, A. Grattoni, D. Fine, F. Hussain, M. Ferrari, J. Phys. Chem. B 114 (2010) 11117.
[24] V. Noinville, C. Vidalmadjar, B. Sebille, J. Phys. Chem. 99 (1995) 1516.
[25] S. Ravichandran, J.D. Madura, J. Talbot, J. Phys. Chem. B 105 (2001) 3610.
[26] R. Karnik, K. Castelino, C.H. Duan, A. Majumdar, Nano Lett. 6 (2006) 1735.
[27] N.F.Y. Durand, A. Bertsch, M. Todorova, P. Renaud, Appl. Phys. Lett. 91 (2007).
[28] N.F.Y. Durand, C. Dellagiacoma, R. Goetschmann, A. Bertsch, I. Marki, T. Lasser, P. Renaud, Anal. Chem. 81 (2009) 5407.
[29] H.-J. Limbach, A. Arnold, B.A. Mann, C. Holm, Comput. Phys. Commun. 174 (2006) 704.
[30] W. Humphrey, A. Dalke, K. Schulten, J. Molec, Graphics 14 (1996) 33.